JOC Article

$^4J_{COCCH}$ and $^4J_{CCCCH}$ as Probes of Exocyclic Hydroxymethyl Group Conformation in Saccharides

Qingfeng Pan,[†] Thomas Klepach,[†] Ian Carmichael,[‡] Meredith Reed,[§] and Anthony S. Serianni*,[†]

Department of Chemistry and Biochemistry and the Radiation Laboratory, University of Notre Dame, Notre Dame, Indiana 46556, and Omicron Biochemicals, Inc., South Bend, Indiana 46615

serianni.1@nd.edu

Received March 29, 2005

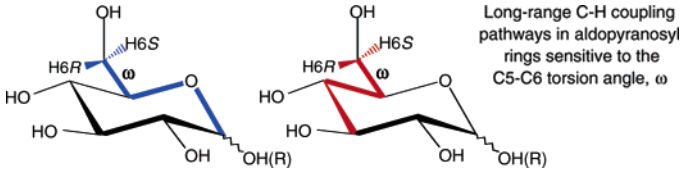

^{1}H NMR spectra of aldohexopyranosyl rings containing ^{13}C-enrichment at either C1 or C3 reveal the presence of long-range $^4J_{C1,H6R/S}$ and $^4J_{C3,H6R/S}$ whose magnitudes depend mainly on the O5−C5−C6−O6 torsion angle. Using theoretical calculations (density functional theory, DFT; B3LYP/6-31G*) and conformationally constrained experimental model compounds, the magnitudes and signs of $^4J_{C1,H6R/S}$ and $^4J_{C3,H6R/S}$ have been established, and their dependencies on the geometry of the C1−O5−C5−C6−H6*R*/*S* and C3−C4−C5−C6−H6*R*/*S* coupling pathways, respectively, were determined. The latter dependencies mimic that observed previously for $^4J_{HH}$ in aliphatic compounds such as propane. DFT calculations also showed that inclusion of non-Fermi contact terms is important for accurate predictions of $^4J_{CH}$ values. Application to methyl α- and β-D-glucopyranosides reveals different rotameric distributions about their hydroxymethyl groups, with the β-anomer enriched in the *gt* rotamer, in agreement with recent multi-*J* redundant coupling analyses. $^4J_{C1,H6R/S}$ and $^4J_{C3,H6R/S}$ are expected to complement other recently developed *J*-couplings for the assignment of hydroxymethyl group conformation in oligosaccharides containing 1,6-glycosidic linkages.

Introduction

Conformational analysis of the exocyclic hydroxymethyl group in saccharides is an important component in evaluating the overall solution conformation of oligosaccharides containing 1,6-linkages (see **1**, Scheme 1).[1,2] Conventional experimental methods are virtually confined to studies of $^3J_{HH}$ between H5 and H6*R*/*S* and subsequent application of Karplus relationships to assign *gg*, *gt*, and *tg* rotamer populations (C5−C6 rotamers; ω) (Scheme 2).[3] However, recent work has shown that the more abundant *J*-couplings involving carbon (J_{CH} and J_{CC} over 1−3 bonds) are sensitive to ω (and in some cases to the C6−O6 torsion angle, θ) (see **2**; Scheme 1) and can be used in conjunction with $^3J_{HH}$ to assign CH_2OH conformation more firmly.[4] These analyses lead not only to the determination of C5−C6 but also C6−O6 rotamer populations in solution, due to the dual dependence of some carbon-based couplings, notably $^2J_{CCH}$, on both ω and θ.

During ongoing NMR studies of ^{13}C-labeled oligosaccharides, we observed that the hydroxymethyl proton resonances of Gal residues were differentially broadened when the residue was enriched with ^{13}C at C1. This observation suggested the presence of an uncharacterized long-range $^4J_{COCCH}$ whose magnitude might depend on C5−C6 bond conformation. This report describes experimental and computational studies aimed at characterizing $^4J_{COCCH}$ (and $^4J_{CCCCH}$) in saccharides (e.g., **3**−**14**, Scheme 3) and discusses potential applications of these uncommon couplings.

[†] Department of Chemistry and Biochemistry, University of Notre Dame.
[‡] Radiation Laboratory, University of Notre Dame.
[§] Omicron Biochemicals, Inc.

(1) Woods, R. J.; Pathiaseril, A.; Wormald, M. R.; Edge, C. J.; Dwek, R. A. *Eur. J. Biochem.* **1998**, *258*, 372−386.
(2) Wormald, M. R.; Petrescu, A. J.; Pao, Y.-L.; Glithero, A.; Elliott, T.; Dwek, R. A. *Chem. Rev.* **2002**, *102*, 371−386.
(3) Stenutz, R.; Carmichael, I.; Widmalm, G.; Serianni, A. S. *J. Org. Chem.* **2002**, *67*, 949−958.
(4) Thibaudeau, C.; Stenutz, R.; Hertz, B.; Klepach, T.; Zhao, S.; Wu, Q.; Carmichael, I.; Serianni, A. S. *J. Am. Chem. Soc.* **2004**, *126*, 15668−15685.

10.1021/jo050615k CCC: $30.25 © 2005 American Chemical Society
Published on Web 07/28/2005

SCHEME 1

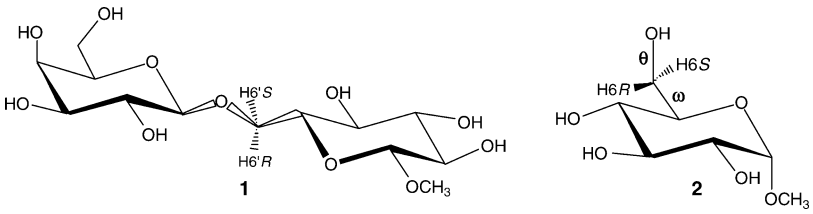

SCHEME 2. Idealized Staggered Rotamers about the C5−C6 Bond of Aldohexopyranosyl Rings

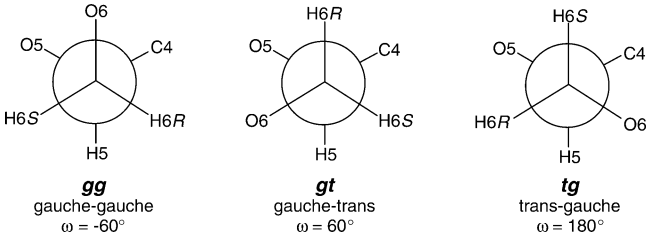

Results and Discussion

General Observations. A comparison of the H6 and H6′ signals[5] in ^{1}H NMR spectra of methyl β-D-galactopyranosyl-(1→6)-β-D-glucopyranoside and methyl β-D-[1-^{13}C]galactopyranosyl-(1→6)-β-D-glucopyranoside **13** (Figure 1) shows that the more shielded Gal H6′ quartet is broadened significantly in **13** relative to the less shielded Gal H6 quartet. Resonance line widths (Figure 1B) show a differential broadening of ∼0.8 Hz, suggesting the presence of a four-bond (C−O−C−C−H) *J*-coupling between C1 and H6′ ($^4J_{C1,H6'}$).

To determine whether the coupling behavior in **13** is generally observed in β-Gal residues, methyl β-D-galactopyranoside and methyl β-D-[1-^{13}C]galactopyranoside **3** were examined. The results revealed a differential H6′ signal broadening (∼0.6 Hz) similar to that observed in **13** (Table 1, Figure 2). Differential broadening was also observed in methyl β-D-[1-^{13}C]galactopyranosyl-(1→4)-β-D-xylopyranoside **12** (Figure S1, Supporting Information). In contrast, no or little differential H6 or H6′ signal broadening was observed when methyl α-D-glucopyranoside and methyl α-D-[1-^{13}C]glucopyranoside **14** were compared (Table 1, Figure S2). However, a smaller but clearly observable selective broadening of the H6 signal in methyl β-D-[1-^{13}C]glucopyranoside **7** was observed (Figure S3). These results suggested that rotational preferences about the C5−C6 bond influence the magnitude of the putative $^4J_{CH}$. Recent multi-*J*-coupling analysis[4] and prior work[6,7] have shown that hydroxymethyl rotamer populations in *gluco* and *galacto* configurations differ considerably. Orientation of the C4−O4 bond induces different relative stabilities of the *gg*,

TABLE 1. Disposition[a] of the C6−H6*R* and C6−H6*S* Bonds with Respect to the C1−O5−C5−C6−H6*R*/*S* and C3−C4−C5−C6−H6*R*/*S* Coupling Pathways in Specific Hydroxymethyl Rotamers, and Experimental Line Width Difference[b] of H6*R*/*S* in 3/4, 7/8, and 14

	C6−H6R			C6−H6S			
compound	*gg*	*gt*	*tg*	*gg*	*gt*	*tg*	$LW_{H6R} - LW_{H6S}$
Me β-[1-^{13}C]Gal **3**	IP	OP	OP	OP	IP	OP	∼0.6
Me β-[3-^{13}C]Gal **4**	OP	OP	IP	IP	OP	OP	nb
Me β-[1-^{13}C]Glc **7**	IP	OP	OP	OP	IP	OP	∼0.4
Me β-[3-^{13}C]Glc **8**	OP	OP	IP	IP	OP	OP	nb
Me β-[1-^{13}C]Glc **14**	IP	OP	OP	OP	IP	OP	nb

[a] IP = in-plane, OP = out-of-plane. [b] In Hz ± 0.1 Hz, ^2H_2O solvent, 25 °C. LW = line width (see Experimental Section); nb = no broadening observed (line width difference <0.2 Hz).

SCHEME 3

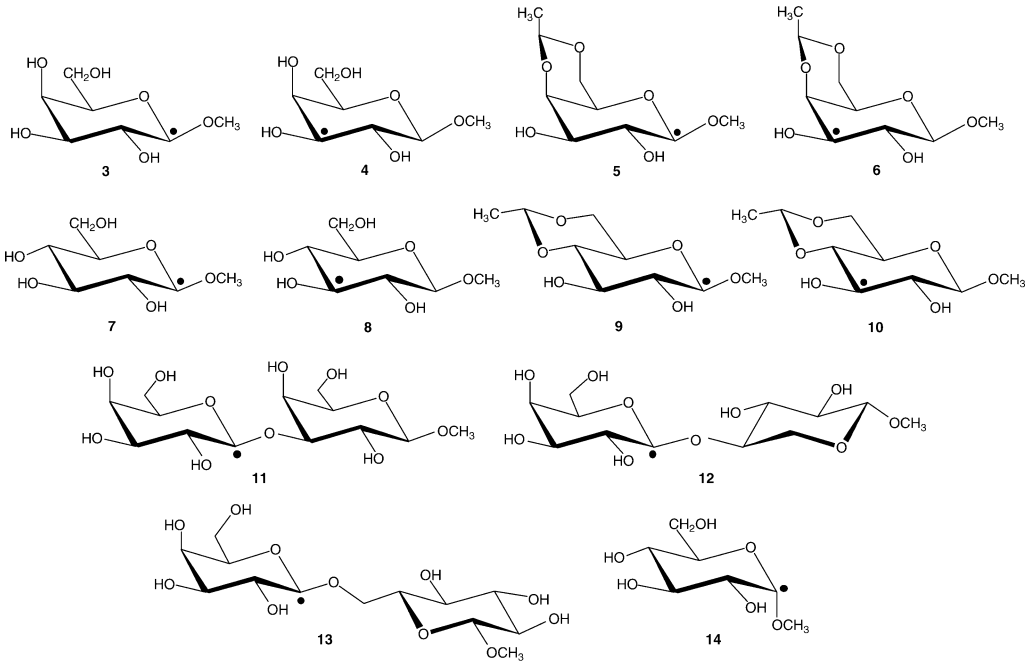

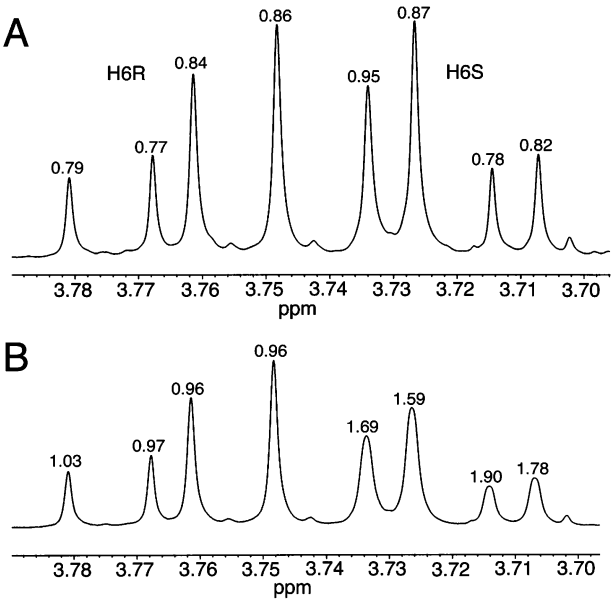

FIGURE 1. (A) Partial 600-MHz ^{1}H NMR spectrum of methyl β-D-galactopyranosyl-(1→6)-β-D-glucopyranoside in ^2H_2O showing resonance line widths of the H6*R* and H6*S* signals of the Gal residue. The ratio of the average line widths of both signals (H6*S*/H6*R*) = 1.05, and the average difference in line width (H6*S* − H6*R*) = 0.04 Hz. (B) Same spectrum in (A) for **13**. The ratio of the average line widths of both signals = 1.78, and the average difference in line width = 0.76 Hz.

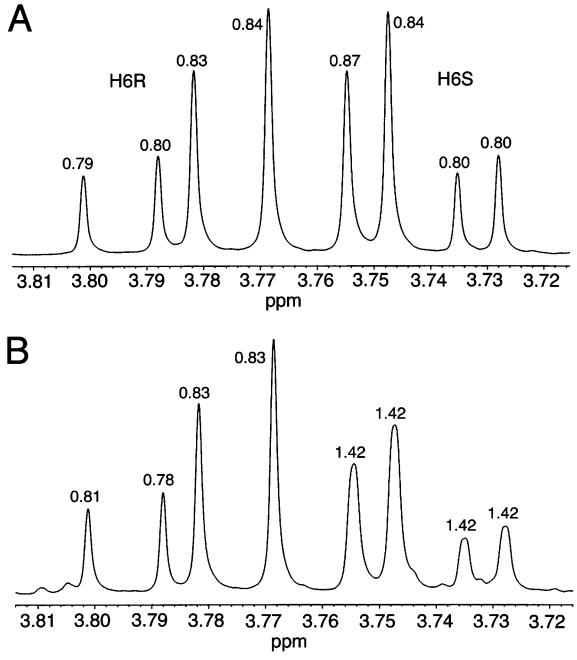

FIGURE 2. (A) Partial 600-MHz ^{1}H NMR spectrum of methyl β-D-galactopyranoside in ^2H_2O showing resonance line widths of the H6*R* and H6*S* signals. The ratio of the average line widths of both signals (H6*S*/H6*R*) = 1.01, and the average difference in line width (H6*S* − H6*R*) = 0.01 Hz. (B) Same spectrum in (A) for **3**. The ratio of the average line widths of both signals = 1.75, and the average difference in line width = 0.61 Hz.

gt, and *tg* rotamers (Scheme 2) due, in part, to destabilizing 1,3-diaxial effects. In **14**, *gg* and *gt* are nearly equally populated (∼40% and ∼53%, respectively), and the *tg* population is negligible (∼7%).[4] In **7**, *gg* ≈ 31%, *gt* ≈ 61%, and *tg* ≈ 8%.[4] In **3**, *gt* ≈ 73% and *tg* ≈ 25%, and the *gg* population is very small (∼0%).[4]

Stereospecific assignments[8] of the diastereotopic H6 and H6′ of **3**, **7**, and **14** have shown that H6*S* is downfield of H6*R* in *gluco* (**7**, **14**), and H6*R* is downfield of H6*S* in *galacto* (**3**). Thus, in **3**, the upfield hydroxymethyl proton (H6′) that exhibits the putative coupling to C1 is H6*S*. H6*S* in **3** is *anti* to O5 in *gt* (i.e., in-plane with respect to C1) and *gauche* to O5 in *tg* (i.e., out-of-plane with respect to C1) (Table 1). H6*R* is out-of-plane with respect to C1 in both *gt* and *tg*. Since *gg* is minimally populated in **3**, its contribution to the observed coupling can be ignored. If an in-plane (zigzag) orientation (i.e., C1−O5−C5−C6 and O5−C5−C6−H6R/S torsions of ∼180°) is required to observe the coupling, then H6*R* should experience little or no coupling to C1, whereas H6*S* should be coupled.

In **7** and **14**, H6*S* is out-of-plane in *gg* and in-plane in *gt*, whereas H6 is out-of-plane in *gt* and in-plane in *gg*. The small contribution by *tg* is ignored. Thus, coupling effects are equivalent for both H6*R* and H6*S* in *gluco* structures in which *gg* and *gt* are equally favored (i.e., **14**), and no differential broadening is observed (Figure S2). Interestingly, in **7**, the favored *gt* rotamer (∼61%) leads to a small differential broadening (∼0.3 Hz) of the H6*S* signal (Table 1, Figure S3).

Theoretical Studies of $^4J_{CH}$ Structural Dependencies. Since the above arguments rest on the assumption that a coplanar C1−O5−C5−C6−H6*R*/*S* arrangement is required to observe the putative long-range coupling, the effect of pathway geometry was evaluated by calculating $^4J_{C1,H6R/S}$ in model structures **15**−**18** using density functional theory (DFT). Calculations of $^4J_{C3,H6R/S}$ were also conducted. These results are shown in Figure 3.

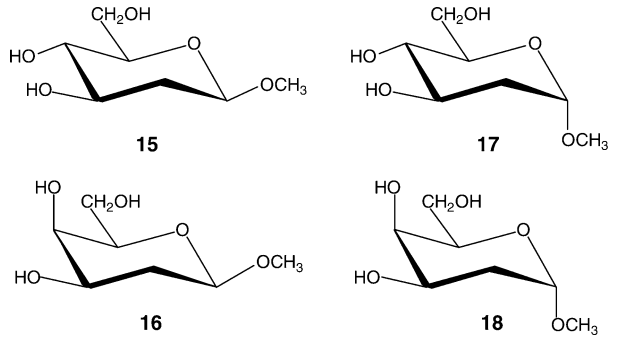

As anticipated, $^4J_{C1,H6R/S}$ is larger (i.e., more positive) for the coplanar C1−O5−C5−C6−H6*R*/*S* pathway

(5) H6 is defined as the less shielded, and H6′ the more shielded, diastereotopic proton on C6.

(6) (a) Marchessault, R. H.; Perez, S. *Biopolymers* **1979**, *18*, 2369−2374. (b) Rockwell, G. D.; Grindley, T. B. *J. Am. Chem. Soc.* **1998**, *120*, 10953−10963. (c) Kuttel, M.; Brady, J. W.; Naidoo, K. J. *J. Comput. Chem.* **2002**, *23*, 1236−1243. (d) Behrends, R.; Cowman, M. K.; Eggers, F.; Eyring, E. M.; Kaatze, U.; Majewski, J.; Petrucci, S.; Richmann, K.-H.; Riech, M. *J. Am. Chem. Soc.* **1997**, *119*, 2182−2186.

(7) Bock, K.; Duus, J. O. *J. Carbohydr. Chem.* **1994**, *13*, 513−543. (b) Nishida, Y.; Hori, H.; Ohrui, H.; Meguro, H. *J. Carbohydr. Chem.* **1988**, *7*, 239−250.

(8) (a) Ohrui, H.; Nishida, Y.; Higuchi, H.; Hori, H.; Meguro, H. *Can. J. Chem.* **1987**, *65*, 1145−1153. (b) Ohrui, H.; Nishida, Y.; Meguro, H. *Agric. Biol. Chem.* **1984**, *48*, 1049−1053. (c) Hori, H.; Nakajima, Y.; Nishida, H.; Ohrui, H.; Meguro, H. *J. Carbohydr. Chem.* **1986**, *5*, 585−600.

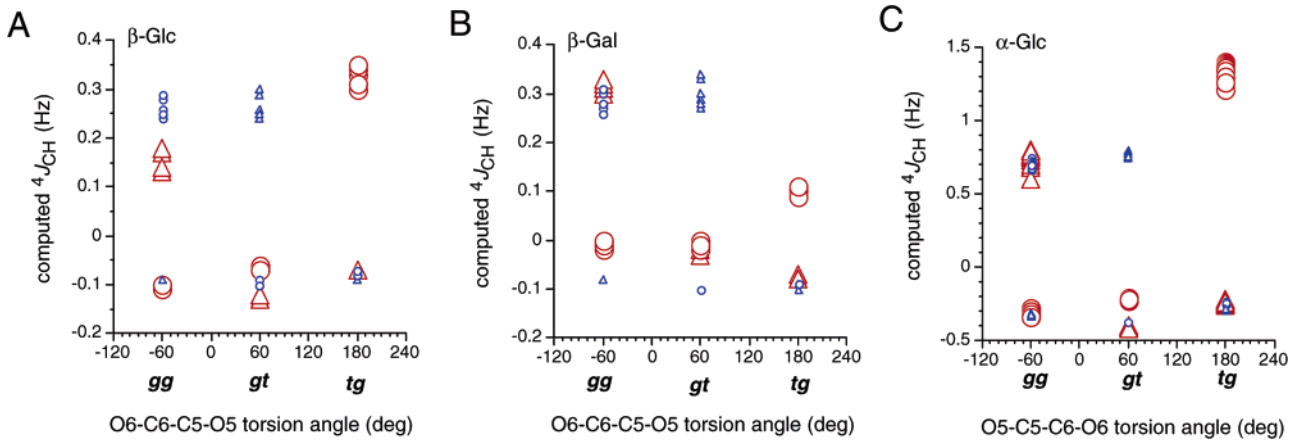

FIGURE 3. (A) Effect of the O6−C6−C5−O5 torsion angle (perfectly staggered rotamers) on $^4J_{C1,H6R/S}$ and $^4J_{C3,H6R/S}$ in **15**: (small blue circles) $^4J_{C1,H6R}$; (small blue triangles) $^4J_{C1,H6S}$; (large red circles) $^4J_{C3,H6R}$; (large red triangles) $^4J_{C3,H6S}$. (B) Same data as in (A) for **16**. Couplings in A and B were computed by DFT methods that neglect non-Fermi contact terms (see Calculations). (C) Same data as in (A) for **17**, calculated using *Gaussian*03 in which both Fermi and non-Fermi contact contributions are included (see Calculations).

geometry, as shown by the calculated coupling to H6*R* in *gg* and H6*S* in *gt* of **15** and **16** (ca. +0.3 Hz) (Figure 3A,B). The effect of C4 configuration on $^4J_{C1,H6R/S}$ appears to be minimal. Likewise, $^4J_{COCCH}$ involving H6*S* in *gg*, H6*R* in *gt*, and H6*R/S* in *tg* show minimal coupling (ca. −0.1 Hz) in **15** and **16**; these pathway geometries lack the required coplanarity. The spread of points in Figure 3A,B is caused by rotations of the C1−O1 and C3−O3 bonds. The effect of these torsions on the computed $^4J_{COCCH}$ is small.

The DFT results for $^4J_{C3,H6R/S}$ are more complex (Figure 3A,B). Here, 1,3-effects are evident. In *gg*, coupling to H6*S* in **16** (∼0.3 Hz) is considerably larger than to H6*S* in **15** (0.15 Hz) even though both protons lie in the C3−C4−C5−C6−H6*S* coupling plane. Comparably, in *tg*, coupling to H6*R* in **15** is larger (∼0.35 Hz) than to H6*R* in **16** (∼0.1 Hz), even though both share the coplanar arrangement. Apparently, configuration at the intervening C4 carbon along the C3−C4−C5−C6−H6*R/S* pathway effects $^4J_{CH}$, with a 1,3-diaxial orientation of O4 and O6 enhancing the coupling. For out-of-plane couplings, trends are less clear, although there is indication that 1,3-effects are also present (e.g., note the slightly larger coupling to H6*R* in **16** in *gg* compared to H6*R* in **15**).

Rotation of the C1−O1 bond modulates stereoelectronic effects at the anomeric center, and thus might modulate $^4J_{C1,H6R/S}$ values. This possibility was studied in the α-Glc (**17**) and α-Gal (**18**) configurations (Figures S4 and S5). $^4J_{C1,H6R/S}$ in both configurations is slightly affected by C1−O1 bond rotation (± 0.05 Hz) for in-plane geometries, but very little effect was observed for the out-of-plane geometries. As a control, the effect of C1−O1 rotation on $^4J_{C3,H6R/S}$ was evaluated and found to be negligible (Figures S4B and S5B).

A comparison between data in Figure 3 and Figures S4 and S5 shows that anomeric configuration does not affect $^4J_{C1,H6R/S}$ and $^4J_{C3,H6R/S}$ significantly;[9a] that is, similar absolute couplings and coupling trends are observed when identical C5−C6 rotamers are compared.

The effect of C3−O3 bond rotation on $^4J_{C1,H6R/S}$ and $^4J_{C3,H6R/S}$ in **17** was found to be negligible (Figure S6). Comparison of these data to those in Figures S4 and S5 supports the conclusion that stereoelectronic effects are the probable cause of the small but periodic dependence of $^4J_{C1,H6R/S}$ on C1−O1 bond rotation. A small effect on $^4J_{C1,H6R/S}$ is observed in **17** when the C3−O3 bond is rotated, but the effect exhibits a periodicity and amplitude different than those observed in Figure S4A. The effect of C3−O3 bond rotation on $^4J_{C3,H6R/S}$ in **17** is small (Figure S6B).

The above calculations show that (a) a coplanar geometry is essential for the observation of $^4J_{C1,H6R/S}$ or $^4J_{C3,H6R/S}$, (b) the dynamic ranges of $^4J_{C1,H6R/S}$ and $^4J_{C3,H6R/S}$ are similar, and (c) configuration at the intervening C4 along the $^4J_{C3,H6R/S}$ coupling pathway influences *J* magnitude, with 1,3-diaxial effects enhancing the coupling. Both positive and negative $^4J_{CH}$ signs are predicted, but the small coupling magnitudes and the known uncertainties in the calculations render this sign information unreliable (see below).

DFT computations that recover only the Fermi contact contribution to $^4J_{CH}$ (Figure 3A,B) yield maximal positive couplings of 0.3−0.4 Hz, which are considerably smaller than those observed experimentally in both constrained and unconstrained molecules (Tables 1 and 2). While some of the discrepancy might originate from present limitations of the DFT method, it is also possible that non-Fermi contact contributions to $^4J_{CH}$ are not negligible. To evaluate this possibility, $^4J_{CH}$ values were calculated in **17** using *Gaussian*03, which yielded computed couplings containing both the Fermi and non-Fermi contact contributions (Figure 3C). The general trends observed in Figure 3A are maintained in Figure 3C, but curve amplitude is greater in the *Gaussian*03 treatment, giving coplanar couplings in better agreement with experimental values.

The effect of C5−C6 bond rotation in **15** on $^4J_{C1,H6R/S}$ and $^4J_{C3,H6R/S}$ was evaluated by DFT using *Gaussian*03.

(9) (a) The conclusion that anomeric configuration does not influence the magnitude of $^4J_{C1,\ H6R/S}$ significantly was tested by measuring $^4J_{C1,H6R}$ in methyl 4,6-*O*-ethylidene-α-D-[1-^{13}C]galactopyranoside. The observed coupling (1.0 Hz) is similar to that observed in **5** (see Table 2). (b) Bock, K.; Pedersen, C. *Acta Chem. Scand.* **1977**, *B31*, 354−358. (c) Podlasek, C. A.; Wu, J.; Stripe, W. A.; Bondo, P. B.; Serianni, A. S. *J. Am. Chem. Soc.* **1995**, *117*, 8635−8644.

TABLE 2. Disposition[a] of C6−H6*R* and C6−H6*S* Bonds with Respect to C1−O5−C5−C6−H6*R/S* and C3−C4−C5−C6−H6*R/S* Coupling Pathways and Experimental[b] $^4J_{C1,H6R/S}$ and $^4J_{C3,H6R/S}$ in 5/6 and 9/10

compound	C6−H6*R*	C6−H6*S*	$^4J_{C1,H6R}$	$^4J_{C1,H6S}$	$^4J_{C3,H6R}$	$^4J_{C3,H6S}$
β-[1-^{13}C]E-Gal **5**	IP	OP	1.1	nc[c]		
β-[3-^{13}C]E-Gal **6**	OP	IP			nc	1.7
β-[1-^{13}C]E-Glc **9**	OP	OP	nc	nc		
β-[3-^{13}C]E-Glc **10**	IP	OP			1.3	nc

[a] IP = in-plane, OP = out-of-plane. [b] In Hz ± 0.1 Hz, ^2H_2O solvent, 25 °C. [c] nc = no coupling observed (J < 0.5 Hz)

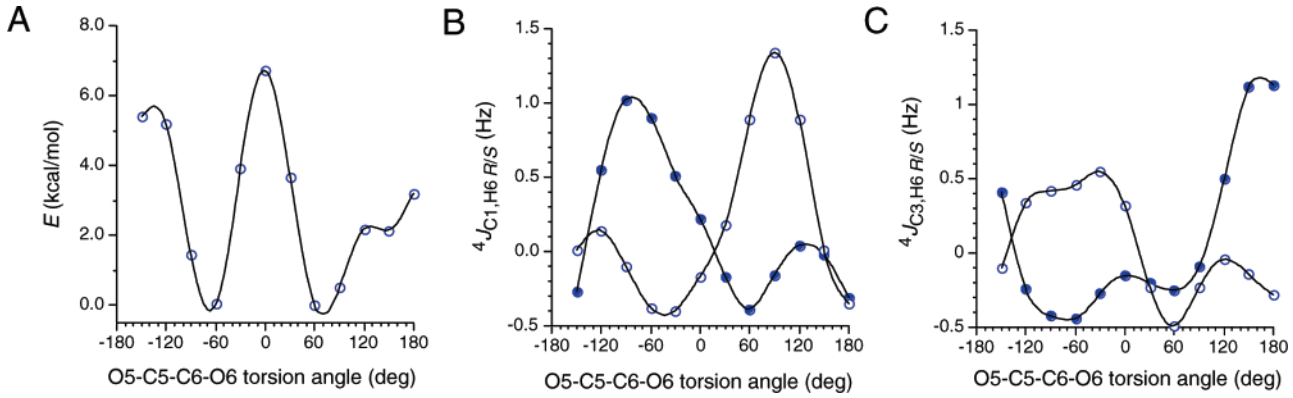

FIGURE 4. (A) The dependence of total energy of **15** on the O5−C5−C6−O6 torsion angle (*Gaussian*03). (B) Dependence of $^4J_{C1,H6R}$ (closed blue circles) and $^4J_{C1,H6S}$ (open blue circles) on the O5−C5−C6−O6 torsion angle in **15** (*Gaussian*03). (C) Dependence of $^4J_{C3,H6R}$ (closed blue circles) and $^4J_{C3,H6S}$ (open blue circles) on the O5−C5−C6−O6 torsion angle in **15** (*Gaussian*03).

Total energy plotted as a function of C5−C6 bond rotation (Figure 4A) shows roughly equal energies for the *gg* and *gt* rotamers, and higher energy for *tg*, in good agreement with distributions in solution determined by NMR. The $^4J_{CH}$ plots (Figure 4B,C) confirm the importance of the coplanar coupling pathway in eliciting an observed coupling. Discrete couplings determined for perfectly staggered O5−C5−C6−O6 rotamers can be compared to those shown in Figure 3A. As observed in **17** (Figure 3C), DFT-computed couplings are larger in **15** when non-Fermi contact terms are included in the calculation.

Experimental Validations Using Constrained Compounds. The DFT results were validated experimentally, and additional questions were addressed, using 4,6-*O*-ethylidene derivatives of **3** and **7** prepared with ^{13}C-enrichment at either C1 or C3 (**5**, **6**, **9** and **10**). These derivatives contain constrained O5−C5−C6−O6 torsion angles, providing C1−O5−C5−C6−H6*R/S* and C3−C4−C5−C6−H6*R/S* coupling pathways of known geometry from which limiting experimental $^4J_{CH}$ were obtained (Table 2). In **5**, the in-plane C1−O5−C5−C6−H6*R* pathway yielded a $^4J_{C1,H6R}$ = 1.1 Hz (Figure 5B).[9a] In **6**, the in-plane C3−C4−C5−C6−H6*S* pathway gave $^4J_{C3,H6S}$ = 1.7 Hz (Figure 5C), while in **10**, the in-plane C3−C4−C5−C6−H6*R* pathway gave $^4J_{C3,H6R}$ = 1.3 Hz (Figure S7). Couplings were not observed for the out-of-plane pathways.

The DFT calculations predict positive signs of $^4J_{CCCCH}$ and $^4J_{COCCH}$ for coplanar coupling pathways. This prediction was tested experimentally by determining the signs of $^4J_{C1,H6R}$ in **5** and $^4J_{C3,H6R}$ in **10**. Signs were determined by observing the relative displacements of the dual H1 and H3 cross-peaks in **5** and **10**, respectively, in ^{1}H−^{1}H TOCSY spectra (Figure 6). For **5**, the displacements were calibrated using the H3 and H5 correlations, which contain $^3J_{C1,H3}$ and $^3J_{C1,H5}$ that are expected to be positive (Figure 6B); the opposite displacement observed for the H2 correlations indicates that $^2J_{C1,H2}$ is negative, consistent with prior work.[9b,c] Using this internal calibration, $^4J_{C1,H6R}$ in **5** was found to be positive (Figure 6C). Likewise, analysis of the ^{1}H−^{1}H TOCSY spectrum of **10** (Figure S8) revealed a positive sign for $^4J_{C3,H6R}$; in this case, the internal reference was $^2J_{C1,H2}$, which is known to be negative.[9b,c]

Signal assignments for H6*R* and H6*S* in **9/10** are straightforward on the basis of the very different values of $^3J_{H5,H6R}$ and $^3J_{H5,H6S}$ (see Experimental Section). These couplings, however, are very similar in **5/6**, making stereospecific assignments difficult. Observation of the long-range $^4J_{C1,H6R}$ in **5/6** can be used to make these assignments. This application would involve circular reasoning if the structural dependencies of $^4J_{CH}$ could not be independently verified. However, the DFT calculations and studies of model compounds provide this verification, thus placing the argument on firmer ground.

Conclusions

Long-range J-couplings between C1 or C3 and the H6*R/S* hydroxymethyl protons of aldohexopyranosyl rings can be observed in solution when certain conformational conditions are fulfilled. These couplings are maximal (1.2−1.7 Hz) when the two central dihedral angles within the C1−O5−C5−C6−H6*R/S* or C3−C4−C5−C6−H6*R/S* fragment are ∼180° (i.e., the constituent C1−O5−C5−C6 and O5−C5−C6−H6*R/S* dihedral angles are ∼180°). These 180°/180° (in-plane) couplings are positive in sign. Dihedral angle combinations of 180°/60° and 180°/−60° yield smaller, presumably negative, couplings. Since one of the two dihedral angles is fixed by the pyranosyl ring at ∼180° in the systems examined, the dependency of $^4J_{CH}$ on the full 360° rotation of both dihedrals was not explored.

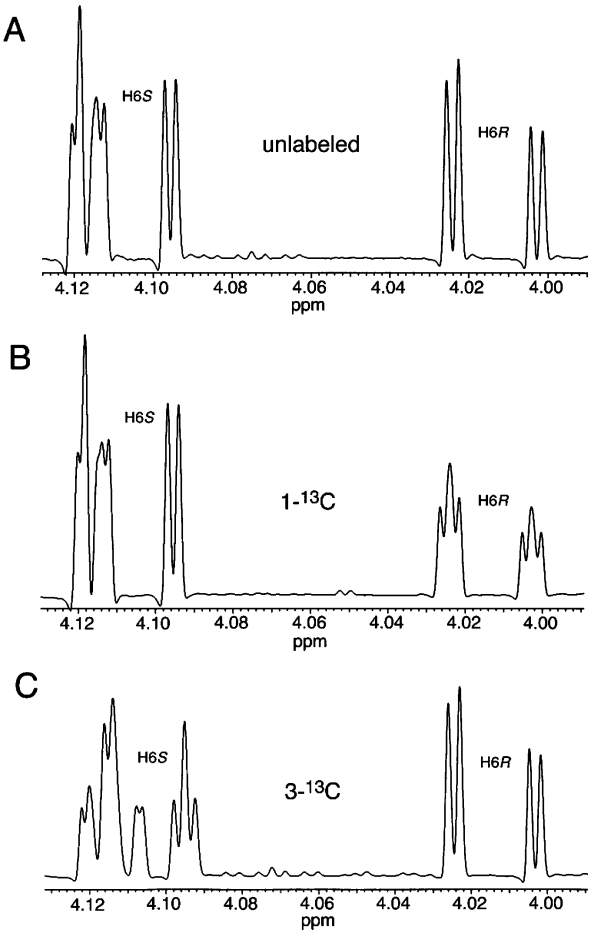

FIGURE 5. (A) Partial 600-MHz ^{1}H NMR spectrum of methyl 4,6-*O*-ethylidene-β-D-galactopyranoside in ^2H_2O. Only the upfield half of the H6*S* signal is cleanly observed; the downfield component overlaps the H4 signal at ~4.12 ppm. (B) Same spectrum as in (A) for **5**, showing splitting of the H6*R* quartet by ^{13}C at C1 ($^4J_{C1,H6R}$). (C) Same spectrum as in (A) for **6**, showing splitting of the H6*S* quartet by ^{13}C at C3 ($^4J_{C3,H6S}$).

DFT-computed $^4J_{C1,H6R/S}$ and $^4J_{C3,H6R/S}$ values are affected significantly by the inclusion of non-Fermi contact terms in the calculation. Inclusion of the latter yielded more positive in-plane couplings, in better agreement with experimental data. Experimental measurements of $^4J_{CH}$ signs for in-plane geometries confirmed the positive sign predicted by DFT. Negative couplings were predicted by DFT for the 180°/60° and 180°/−60° conformations regardless of whether non-Fermi terms were included or excluded in the calculation.

The DFT calculations of *J*-couplings reported herein were conducted in vacuo. Better agreement between experiment and theory was obtained when non-Fermi (NF) contact contributions were included in these calculations. Given the small magnitudes of $^4J_{CH}$ values, inclusion of the NF terms, which can be computed reliably, is highly desirable. The effects of solvent on $^4J_{CH}$ may also contribute to the observed differences, but these effects cannot be calculated reliably at present. However, preliminary results show that solvent effects drop off significantly as coupling pathway lengthens, that is, the effects are much larger for $^1J_{CH}$ than for $^2J_{CH}$ and $^3J_{CH}$, the latter being <0.2 Hz. These results suggest that the solvent effect on $^4J_{CH}$ is small and thus probably does not account for the observed differences between experiment and theory when only the Fermi contact terms were included in the calculations.

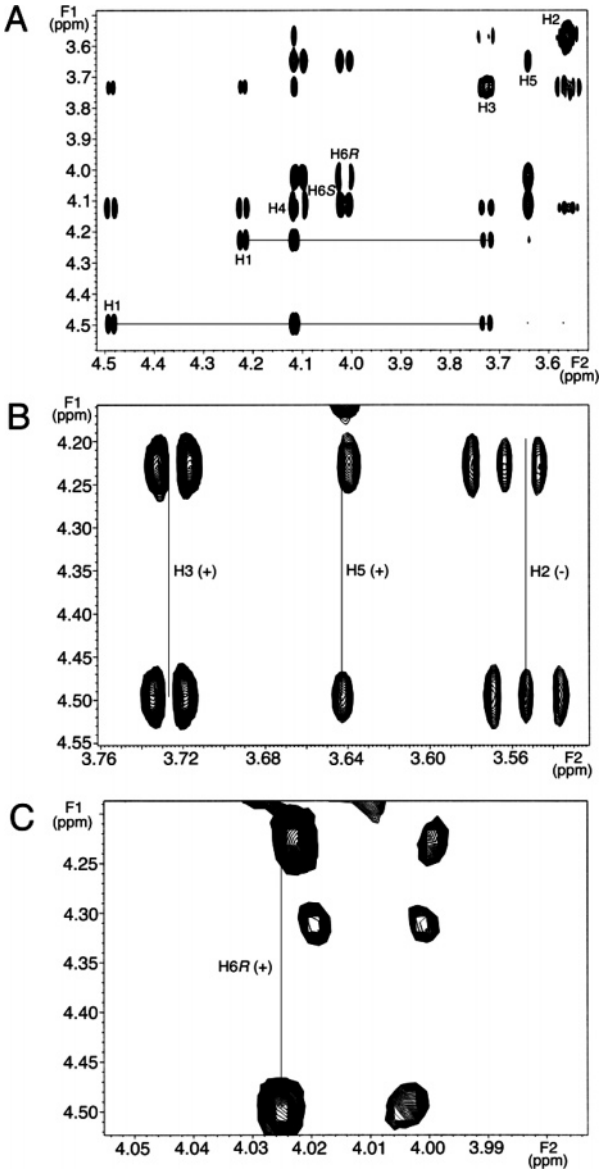

FIGURE 6. (A) ^{1}H−^{1}H TOCSY spectrum of **5** (600 MHz) in ^2H_2O showing signal assignments along the diagonal and the location of paired H1 cross-peaks used to determine coupling signs. (B) Expanded region of (A) showing the H1/H2, H1/H3 and H1/H5 correlations (these signals are comparatively weak and thus not observed in (A) at the signal threshold used for plotting). The observed signal displacements are due to $^2J_{C1,H2}$ (−), $^3J_{C1,H3}$ (+) and $^3J_{C1,H5}$ (+). The vicinal couplings show displacements having an opposite sense to that associated with the geminal coupling, indicating their different signs. (C) Expanded region of (A) showing the H1/H6*R* correlations. Comparison to the reference displacements shown in (B) indicates that $^4J_{C1,H6R}$ is (+).

The results of pioneering studies of $^4J_{HH}$ by Barfield and co-workers[10] in aliphatic systems (e.g., propane) show a close correspondence to the observed behavior of $^4J_{CH}$ in aldopyranosyl rings. The H−C−C−C−H coupling

(10) Barfield, M.; Dean, A. M.; Fallick, C. J.; Spear, R. J.; Sternwell, S.; Westerman, P. W. *J. Am. Chem. Soc.* **1975**, *97*, 1482−1492.

pathway in propane yielded small positive $^4J_{HH}$ (~2 Hz) for the in-plane geometry, which dropped to a negative value (ca. −0.4 Hz) for the 180°/60° (or the equivalent 180°/−60°) combination. Thus, a correlation appears to exist between $^4J_{CH}$ and $^4J_{HH}$ which is similar to the known correlation between $^3J_{CH}$ and $^3J_{HH}$.[11]

The existence of complementary $^4J_{C1,H6R/S}$ and $^4J_{C3,H6R/S}$ in aldohexopyranosyl rings provides a means to assign stereochemically the CH_2OH proton signals in ^1H NMR spectra and a potential new probe of exocyclic CH_2OH conformation in solution. In the latter respect, these long-range couplings can be used in conjunction with other redundant *J*-couplings[3,4] to assess conformation. Both applications may be advantageous in structural NMR studies of ^{13}C-labeled oligosaccharides containing 1,6-linkages.

The relatively strict geometric requirements for the observation of $^4J_{CH}$ lead to useful insights into CH_2OH conformation when changes in their magnitudes are observed. The sensitivity of these couplings to relatively small changes in C5−C6 rotamer populations is demonstrated by the significantly different $^4J_{CH}$ values observed in **7** and **14**. The enhanced *gt* population in the former results in a discernible selective broadening of the H6*S* signal, whereas no selective broadening is observed in **14**. These data provide new experimental evidence that the distributions of hydroxymethyl rotamers in **7** and **14** are probably not identical, suggesting that anomeric configuration can influence exocyclic CH_2OH conformation.

Experimental Section

Reagents. *o*-Nitrophenol, Sepharose G10, Dowex 1 × 2 (200−400 mesh) (Cl^-) ion-exchange resin, β-galactosidase (E.C. 3.2.1.23) (*E. coli*), *o*-nitrophenyl (ONP) β-D-galactopyranoside, methyl β-D-glucopyranoside, and acetaldehyde dimethylacetal were purchased from commercial suppliers. D-[1-^{13}C]Glucose, D-[3-^{13}C]glucose, D-[1-^{13}C]galactose, and D-[3-^{13}C]galactose were obtained from Omicron Biochemicals, Inc. (South Bend, IN).

Methyl β-D-[1-^{13}C]galactopyranoside **3**, methyl β-D-[3-^{13}C]-galactopyranoside **4**, methyl β-D-[1-^{13}C]glucopyranoside **7**, methyl β-D-[3-^{13}C]galactopyranoside **8**, and methyl α-D-[1-^{13}C]-glucopyranoside **14** were prepared by Fischer glycosidation and purified by chromatography (Dowex 1 × 2 (200−400 mesh) (OH^-)[12a]) as described previously.[9c]

Methyl 4,6-*O*-Ethylidene-D-Aldohexopyranosides. Methyl 4,6-*O*-ethylidene-β-D-[1-^{13}C]galactopyranoside **5**, methyl 4,6-*O*-ethylidene-β-D-[3-^{13}C]galactopyranoside **6**, methyl 4,6-*O*-ethylidene-β-D-[1-^{13}C]glucopyranoside **9**, and methyl 4,6-*O*-ethylidene-β-D-[3-^{13}C]glucopyranoside **10** were prepared from the corresponding ^{13}C-labeled methyl D-aldohexopyranosides according to the following procedure. To a stirred mixture containing methyl glycoside (100 mg, 0.52 mmol) and $CH_3CH(OCH_3)_2$ (65 μL, 1.2 equiv) in DMF (10 mL) at 50 °C was added *p*-toluenesulfonic acid monohydrate (3 mg). The reaction mixture was stirred overnight at 50 °C, and a few drops of triethylamine were added to quench the reaction. The solution was concentrated at 30 °C in vacuo to a minimum volume and loaded on a silica gel column (1 cm × 50 cm), which was eluted with ethyl acetate to yield methyl 4,6-*O*-ethylidene-D-aldohexopyranoside (TLC detection spray reagent: 9 g $Ce(SO_4)_2$ and 22.5 g $(NH_4)_2MoO_4$ in 1 L of 10% H_2SO_4) (~95 mg, ~84%; purity, ~95%). (J_{HH} in **5/6**: H1−H2, 8.0 Hz; H2−H3, 9.9 Hz; H3−H4, 3.8 Hz; H4−H5, 1.1 Hz; H5−H6*R*, 1.8 Hz; H5−H6*S*, 1.7 Hz; H6*R*−H6*S*, −12.8 Hz; H−CH_3, 5.1 Hz. J_{HH} in **9/10**: H1−H2, 8.0 Hz; H2−H3, 9.1 Hz; H3−H4, 9.5 Hz; H4−H5, 9.6 Hz; H5−H6*R*, 5.1 Hz; H5−H6*S*, 10.1 Hz; H6*R*−H6*S*, −10.5 Hz; H−CH_3, 5.1 Hz).

***o*-Nitrophenyl β-D-[1-^{13}C]galactopyranoside (ONP-Gal).** D-[1-^{13}C]Galactose was prepared from D-lyxose and $K^{13}CN$ (Cambridge Isotope Laboratories; 99 atom % ^{13}C) by cyanohydrin reduction, giving D-[1-^{13}C]galactose and D-[1-^{13}C]-talose;[12b,c] these epimers were purified by chromatography on Dowex 50 × 8 (200−400 mesh) (Ca^{2+}),[13] with the *galacto* isomer eluting first. *o*-Nitrophenyl β-D-[1-^{13}C]galactopyranoside (ONP-Gal) was prepared from D-[1-^{13}C]galactose in an overall yield of 30%.[14]

Synthesis of Unlabeled and Labeled Disaccharides via Enzyme-Catalyzed Transglycosylation. Methyl β-D-[1-^{13}C]-galactopyranosyl-(1→3)-β-D-galactopyranoside **11**, methyl β-D-[1-^{13}C]galactopyranosyl-(1→4)-β-D-xylopyranoside **12**, and methyl β-D-[1-^{13}C]galactopyranosyl-(1→6)-β-D-glucopyranoside **13** were prepared by enzyme-catalyzed transglycosylation according to Nilsson[15] (for **11**) or Lopez and Fernandez-Mayoralas[16] (for **12** and **13**) with some modifications.[17] Reactions were conducted with 1.35 g (4.48 mmol) of ONP-Gal and 2.50 g (12.9 mmol) of methyl β-D-galactopyranoside, methyl β-D-glucopyranoside, or methyl β-D-xylopyranoside. After the reaction was quenched, the mixture was concentrated in vacuo at 40 °C to ~45 mL and applied to a column (2.5 cm × 55 cm) of Sepharose G10. Elution with distilled water gave a phenol-sulfuric acid[18] positive peak near the column void. This disaccharide-containing fraction was collected and concentrated to ~35 mL, and the solution was applied to a column (2.5 × 55 cm) of Dowex 1 × 2 (200−400 mesh) (OH^-) ion-exchange resin.[12a] Elution with distilled water (3.8 mL/fraction, 0.8 mL/min) gave three phenol-sulfuric acid positive peaks: For the synthesis of **11**, Peak 1 (unreacted methyl β-D-galactopyranoside), Peak 2 (methyl β-D-galactopyranosyl-(1→6)-β-D-galactopyranoside; reaction byproduct), Peak 3 (**11**); for the synthesis of **12**, Peak 1 (unreacted methyl β-D-xylopyranoside), Peak 2 (**12**); for the synthesis of **13**, Peak 1 (unreacted methyl β-D-glucopyranoside), Peak 2 (**13**). Disaccharides **11**, **12**, and **13** were characterized by ^1H and ^{13}C NMR; ^{13}C chemical shifts were in good agreement with those reported previously.[19]

NMR Spectroscopy. A 600-MHz FT-NMR spectrometer equipped with a 3-mm Nalorac $^{13}C/^1H$ microprobe was used to obtain 1D ^1H and ^{13}C NMR spectra at 25 °C in ^2H_2O, from which J_{CH} values were extracted. Resolution enhancement was applied to the FID prior to Fourier transformation in order to improve the observation of small couplings. Spectral simulation using MacNUTs[20] was used to extract accurate *J*-couplings from spectra exhibiting second-order behavior. Reported *J*-couplings have absolute errors of ±0.1 Hz unless otherwise stated. Resonance line widths were measured from spectra obtained by direct FT of the fid (i.e., no apodization was

(11) Marshall, J. L. *Carbon−Carbon and Carbon−Proton NMR Couplings: Applications to Organic Stereochemistry and Conformational Analysis*; Verlag Chemie International: Deerfield Beach, FL 1983.

(12) (a) Austin, P. W.; Hardy, F. E.; Buchanan, J. C.; Baddiley, J. *J. Chem. Soc.* **1963**, 5350−5353. (b) Serianni, A. S.; Nunez, H. A.; Barker, R. *Carbohydr. Res.* **1979**, *72*, 71−78. (c) Serianni, A. S.; Vuorinen, T.; Bondo, P. B. *J. Carbohydr. Chem.* **1990**, *9*, 513−541.

(13) Angyal, S. J.; Bethell, G. S.; Beveridge, R. J. *Carbohydr. Res.* **1979**, *73*, 9−18.

(14) Conchie, J.; Levvy, G. A. *Methods Carbohydr. Chem.* **1963**, *2*, 335−337.

(15) (a) Nilsson, K. G. I. *Carbohydr. Res.* **1987**, *167*, 95−103. (b) Nilsson, K. G. I. *Carbohydr. Res.* **1988**, *180*, 53−59.

(16) Lopez, R.; Fernandez-Mayoralas, A. *J. Org. Chem.* **1994**, 59, 737−745.

(17) Thibaudeau, C.; Klepach, T.; Zhao, S.; Reed, M.; Carmichael, I.; Serianni, A. S. *J. Am. Chem. Soc.* Manuscript in preparation.

(18) Hodge, J. E.; Hofreiter, B. T. *Methods Carbohydr. Chem.* **1962**, *1*, 380−394.

(19) Bock, K.; Pedersen, C.; Pedersen, H. *Adv. Carbohydr. Chem. Biochem.* **1984**, *42*, 193−225.

(20) *MacNUTs Pro*; Acorn NMR Inc.: Livermore, CA.

applied); reported line widths at 1/2 peak height ($\Delta\nu_{0.5}$) were obtained by fitting the signal digitally using standard NMR software.

J-Coupling sign determinations were made by analysis of the relative displacements of paired cross-peaks in ^{1}H−^{1}H TOCSY spectra[21,22] of **5** and **10** obtained at 600 MHz as described previously.[23,24] Cross-peak displacements associated with couplings of unknown sign ($^4J_{CCCCH}$ or $^4J_{COCCH}$) were calibrated by comparison to displacements associated with couplings of known sign ($^3J_{CCCH}$/$^3J_{COCH}$ (+), or $^2J_{CCH}$ if the sign was known from prior work). TN-TOCSY spectra were recorded at 600 MHz and 298 K; 256−1024 *t*1 increments of 2048 complex points were collected with 16 transients in the hypercomplex mode. TOCSY transfer was achieved with a 28-ms 90° spin-lock pulse (MLEV17) and 80−200 ms mixing times. Prior to Fourier tranformation, zero-filling was applied in F1 and F2 to produce 8K × 1K (or 8K × 4K) matrices apodized with a Gaussian function in both dimensions.

Calculations

Density functional theory (DFT) calculations using the B3LYP functional[25] and the 6-31G* basis set[26] were conducted within *Gaussian*98[27] for geometric optimization of molecular structures as described previously.[28]

Coupling constants ($^4J_{COCCH}$ and $^4J_{CCCCH}$) were calculated by DFT as described previously[28] using a modified version of *Gaussian*94[29] and an extended basis set ([5s2p1d|3s1p])[2] designed to reliably recover the Fermi contact contribution to the coupling. Additional *J*-coupling calculations were also conducted with *Gaussian*03[30] to determine the effect of non-Fermi contact terms on the magnitudes of $^4J_{C1,H6R/S}$ and $^4J_{C3,H6R/S}$. All computed *J*-couplings reported are *unscaled*. Four series of DFT calculations were conducted. In Series 1, DFT calculations (*Gaussian*94) were conducted on **15** and **16**, which represent mimics of the *β-gluco* and *β-galacto* rings, respectively. Within each structure, three perfectly staggered geometries about the C1−O1 bond (defined as the C2−C1−O1−H torsion angle), two about the C3−O3 bond (defined as the C4−C3−O3−H torsion angle, 60 and 180°), and three about the C5−C6 bond (defined as the O5−C5−C6−O6 torsion angle; Scheme 2) were considered (the C5−C4−O4−H and C5−C6−O6−H torsion angles were held constant at 180°), yielding 18 geometrically optimized structures for use in *J*-coupling calculations (see Schemes S1 and S1 in Supporting Information).

In Series 2, DFT calculations (*Gaussian*94) were conducted on **17** and **18**, which represent mimics of the α-*gluco* and α-*galacto* rings, respectively. Within each structure, the C3−O3 (C2−C3−O3−H = 180°) and the C4−O4 (C5−C4−O4−H torsion = 180°) torsions were fixed, and the C1−O1 torsion (O5−C1−O1−H) was varied in 30° increments through 360° in each of the perfectly staggered rotamers about the C5−C6 bond (Scheme 2), yielding 36 geometrically optimized structures for use in *J*-coupling calculations.

In Series 3, $^4J_{C3,H6R/S}$ was calculated in **17** (*Gaussian*03) as a function of the C2−C3−O3−H torsion angle by rotating the latter in 30° increments through 360°. In these calculations, the C2−C1−O1−H, C5−C4−O4−H, and C5−C6−O6−H torsion angles were fixed at 180°.

In Series 4, *J*-coupling calculations were conducted on **15** (*Gaussian*03) in which the O5−C5−C6−O6 torsion angle was varied in 30° increments through 360°, and both $^4J_{C1,H6R/S}$ and $^4J_{C3,H6R/S}$ were calculated. In these calculations, the C2−C1−O1−H, C2−C3−O3−H, C5−C4−O4−H, and C5−C6−O6−H torsion angles were fixed at 180°.

Acknowledgment. This work was supported by grants from Omicron Biochemicals, Inc. of South Bend, IN and the National Institutes of Health (GM) (to A.S.). The Notre Dame Radiation Laboratory is supported by the Office of Basic Energy Sciences of the United States Department of Energy. This is Document no. NDRL-4569 from the Notre Dame Radiation Laboratory.

Supporting Information Available: Ten figures showing differential line-broadening in the ^{1}H spectrum of **12** (Figure S1), lack of differential line-broadening in the ^{1}H spectrum of **14** (Figure S2), differential line-broadening in the ^{1}H spectrum of **7** (Figure S3), the dependence of $^4J_{C1,H6R/S}$ and $^4J_{C3,H6R/S}$ on the O5−C1−O1−H torsion angle in **17** and **18** (Figures S4 and S5), the dependence of $^4J_{C1,H6R/S}$ and $^4J_{C3,H6R/S}$ on the C2−C3−O3−H torsion angle in **17** (Figure S6), observation of long-range $^4J_{CH}$ in ^{1}H spectra of **10** (Figure S7), $^4J_{CH}$ sign determination from the ^{1}H−^{1}H TOCSY spectrum of **10** (Figure S8), the effect of the O5−C1−O1−H torsion angle on the computed total energies of **17** and **18** (Figure S9), and the effect of the C2−C3−O3−H torsion angle in **17** on total energy for the three staggered hydroxymethyl group rotamers (*gg*, *gt*, and *tg*) (Figure S10). Table S1 contains a list of $^nJ_{CH}$ values (n = 1−3) observed in **3**−**10** and **14**. Schemes S1 and S2 show optimized geometries for **15** and **16**, respectively, used to generate *J*-couplings in the Series 1 calculations (see Calculations). This material is available free of charge via the Internet at http://pubs.acs.org.

JO050615K

(21) Braunschweiler, L.; Ernst, R. R. *J. Magn. Reson*. **1983**, *53*, 521−528.
(22) Bax, A.; Davis, D. G. *J. Magn. Reson*. **1985**, *65*, 355−
(23) Montelione, G. T.; Winkler, M. E.; Rauenbuehler, P.; Wagner, G. *J. Magn. Reson*. **1989**, *82*, 198−204.
(24) Serianni, A. S.; Podlasek, C. A. *Carbohydr. Res.* **1994**, *259*, 277−282.
(25) Becke, A. D. *J. Chem. Phys.* **1993**, *98*, 5648−5652.
(26) Hehre, W. J.; Ditchfield, R.; Pople, J. A. *J. Chem. Phys.* **1972**, *56*, 2257−2261.
(27) Frisch, M. J.; Trucks, G. W.; Schlegel, H. B.; Scuseria, G. E.; Robb, M. A.; Cheeseman, J. R.; Zakrzewski, V. G.; Montgomery, Jr., J. A.; Stratmann, R. E.; Burant, J. C.; Dapprich, S.; Millam, J. M.; Daniels, A. D.; Kudin, K. N.; Strain, M. C.; Farkas, O.; Tomasi, J.; Barone, V.; Cossi, M.; Cammi, R.; Mennucci, B.; Pomelli, C.; Adamo, C.; Clifford, S.; Ochterski, J.; Petersson, G. A.; Ayala, P. Y.; Cui, Q.; Morokuma, K.; Malick, D. K.; Rabuck, A. D.; Raghavachari, K.; Foresman, J. B.; Cioslowski, J.; Ortiz, J. V.; Baboul, A. G.; Stefanov, B. B.; Liu, G.; Liashenko, A.; Piskorz, P.; Komaromi, I.; Gomperts, R.; Martin, R. L.; Fox, D. J.; Keith, T.; Al-Laham, M. A.; Peng, C. Y.; Nanayakkara, A.; Challacombe, M.; Gill, P. M. W.; Johnson, B.; Chen, W.; Wong, M. W.; Andres, J. L.; Gonzalez, C.; Head-Gordon, M.; Replogle, E. S.; Pople, J. A. *Gaussian98*, Revision A.9; Gaussian, Inc.: Pittsburgh, PA, 1998.
(28) (a) Bose, B.; Zhao, S.; Stenutz, R.; Cloran, F.; Bondo, P. B.; Bondo, G.; Hertz, B.; Carmichael, I.; Serianni, A. S. *J. Am. Chem. Soc.* **1998**, *120*, 11158−11173. (b) Cloran, F.; Carmichael, I.; Serianni, A. S. *J. Am. Chem. Soc.* **1999**, *121*, 9843−9851.
(29) Frisch, M. J.; Trucks, G. W.; Schlegel, H. B.; Gill, P. M. W.; Johnson, B. G.; Robb, M. A.; Cheeseman, J. R.; Keith, T.; Petersson, G. A.; Montgomery, J. A.; Raghavachari, K.; AlLaham, M. A.; Zakrzewski, V. G.; Ortiz, J. V.; Foresman, J. B.; Peng, C. Y.; Ayala, P. Y.; Chen, W.; Wong, M. W.; Andres, J. L.; Replogle, E. S.; Gomperts, R.; Martin, R. L.; Fox, D. J.; Binkley, J. S.; Defrees, D. J.; Baker, J.; Stewart, J. P.; Head-Gordon, M.; Gonzalez, C.; Pople, J. A. *Gaussian94*; Gaussian, Inc.: Pittsburgh, PA, 1995.
(30) Frisch, M. J.; Trucks, G. W.; Schlegel, H. B.; Scuseria, G. E.; Robb, M. A.; Cheeseman, J. R.; Montgomery, Jr., J. A.; Vreven, T.; Kudin, K. N.; Burant, J. C.; Millam, J. M.; Iyengar, S. S.; Tomasi, J.; Barone, V.; Mennucci, B.; Cossi, M.; Scalmani, G.; Rega, N.; Petersson, G. A.; Nakatsuji, H.; Hada, M.; Ehara, M.; Toyota, K.; Fukuda, R.; Hasegawa, J.; Ishida, M.; Nakajima, T.; Honda, Y.; Kitao, O.; Nakai, H.; Klene, M.; Li, X.; Knox, J. E.; Hratchian, H. P.; Cross, J. B.; Adamo, C.; Jaramillo, J.; Gomperts, R.; Stratmann, R. E.; Yazyev, O.; Austin, A. J.; Cammi, R.; Pomelli, C.; Ochterski, J. W.; Ayala, P. Y.; Morokuma, K.; Voth, G. A.; Salvador, P.; Dannenberg, J. J.; Zakrzewski, V. G.; Dapprich, S.; Daniels, A. D.; Strain, M. C.; Farkas, O.; Malick, D. K.; Rabuck, A. D.; Raghavachari, K.; Foresman, J. B.; Ortiz, J. V.; Cui, Q.; Baboul, A. G.; Clifford S.; Cioslowski, J.; Stefanov, B. B.; Liu, G.; Liashenko, A.; Piskorz, P.; Komaromi, I.; Martin, R. L.; Fox, D. J.; Keith, T.; Al-Laham, M. A.; Peng, C. Y.; Nanayakkara, A.; Challacombe, M.; Gill, P. M. W.; Johnson, B.; Chen, W.; Wong, M. W.; Gonzalez, C.; Pople, J. A. *Gaussian*03, Revision A.1; Gaussian, Inc.: Pittsburgh, PA, 2003.